

Collisional cooling of ultracold molecules

Hyungmok Son^{1,2,*}, Juliana J. Park¹, Wolfgang Ketterle¹, Alan O. Jamison¹

¹*Research Laboratory of Electronics, MIT-Harvard Center for Ultracold Atoms, Department of Physics, Massachusetts Institute of Technology, Cambridge, Massachusetts 02139, USA*

²*Department of Physics, Harvard University, Cambridge, Massachusetts 02138, USA*

Since the original work on Bose-Einstein condensation ^{1,2}, quantum degenerate gases of atoms have allowed the quantum emulation of important systems from condensed matter and nuclear physics, as well as the study of novel many-body states with no analog in other fields of physics ³. Ultracold molecules in the micro- and nano-Kelvin regimes promise to bring powerful new capabilities to quantum emulation ⁴ and quantum computing ⁵, thanks to their rich internal degrees of freedom compared to atoms. They also open new possibilities for precision measurement and the study of quantum chemistry ⁶. Quantum gases of atoms were made possible by collision-based cooling schemes, such as evaporative cooling. For ultracold molecules, thermalization and collisional cooling have not been realized. With other techniques such as supersonic jets and cryogenic buffer gases, studies have been limited to temperatures above 10 mK ^{7,8}. Here we show cooling of NaLi molecules at micro- and nano-Kelvin temperatures through collisions with ultracold Na atoms, both prepared in their stretched hyperfine spin states. We find a lower bound on the elastic to inelastic collision ratio between molecules and atoms greater than 50—large enough to support sustained

*Corresponding author (e-mail: hson@g.harvard.edu)

collisional cooling. By employing two stages of evaporation, we increase the phase-space density (PSD) of the molecules by a factor of 20, achieving temperatures as low as 220 nK. The favorable collisional properties of a Na and NaLi mixture show great promise for making deeply quantum degenerate dipolar molecules and suggest the potential for such cooling in other systems.

The full potential of ultracold atoms was not realized until the advent of collision-based cooling methods like evaporative and sympathetic cooling. While atomic systems have recently demonstrated laser-cooling to quantum degeneracy, these schemes still require collisional thermalization^{9,10}. Therefore, there has been much work over the past 15 years¹¹ trying to achieve collisional cooling of ultracold molecules. Buffer gas cooling⁸ cannot push below 100 mK due to the rapidly diminishing vapor pressure of buffer gases at such temperatures. Supersonic expansion⁷ can produce temperatures around 100 mK. Controlled collisions in crossed molecular beams¹² can decrease the laboratory-frame velocity of particles while narrowing the velocity distribution. However, this technique hasn't been demonstrated below ≈ 500 mK. Merged supersonic beams can study collisions at energies equivalent to a temperature of 10 mK¹³.

Cooling below 100 mK calls for trapping molecules in magnetic or electrostatic traps and good collisional properties (i.e., a ratio of elastic to inelastic collisions much greater than 1). Such traps require preparing molecules in weak-field seeking states, which are never the absolute ground state, allowing inelastic state-changing collisions to eject the cold molecules from the trap. A variety of systems have been proposed for evaporative or sympathetic cooling^{11,14–18}. So far,

elastic collisions have been observed clearly in O_2 at temperatures below 1 K²¹ and possibly in OH radicals around 10 mK (ref. ²⁰ corrects the earlier report ¹⁹). For the O_2 case, inelastic collisions prevented thermalization and collisional cooling.

In recent years, assembling molecules from ultracold atoms²² and the direct laser-cooling of molecules^{24–27} have both expanded to new molecules and temperature regimes. These offer the first molecular systems below 100 mK, raising the challenge of collisional cooling in the micro- and nanoKelvin regimes. Optical traps allow trapping of the absolute ground state, which removes the concern of state-changing collisions. However, the great hope for collisional cooling in absolute ground state, chemically stable systems has still not been realized²⁸. Rather, chemically stable molecular species have shown anomalously high inelastic loss rates that preclude collisional cooling, possibly due to collision complex formation²⁹ or interactions with optical trapping beams³⁰.

In this article we observe sympathetic cooling of rovibrational ground-state triplet $^{23}\text{Na}^6\text{Li}$ molecules by ^{23}Na atoms, both prepared in their upper stretched hyperfine spin states (i.e., the states with both nuclear and electronic spins aligned along the magnetic bias field direction). Sympathetic cooling of one atomic species by another has been observed in a variety of ultracold atomic mixtures³¹ but triplet NaLi is an unlikely place to find sufficiently good collisional properties. NaLi has energetically allowed chemical reactions, even in the electronic ground state, and the triplet state we work with has an electronic excitation energy of 0.8 eV or 10,000 K.

Furthermore, theoretical studies on various systems have explored the possibility of sup-

pressing inelastic collisions and reactions by spin-polarization with pessimistic predictions for triplet molecules but more favorable predictions for doublet molecules^{17,32–35}. Nonetheless, we report clear thermalization and sympathetic cooling of triplet NaLi to 220 nK. We observe increases of phase-space density (PSD) by 20-fold, opening the possibility of collisionally cooling to deep quantum degeneracy.

Our experimental setup is summarized in Fig.1. Similarly to our previous work^{23,36}, we produce $\approx 3.0 \times 10^4$ NaLi molecules in the rovibrational ground state of the triplet potential from a mixture of Na and Li atoms (further details in Methods). The present work begins with these molecules and $\approx 1.0 \times 10^5$ Na atoms prepared in the upper stretched hyperfine state (in the low-field basis, $|F, m_F\rangle = |2, 2\rangle$) in a 1D optical lattice of 1596 nm light. Due to the differential polarizability at 1596 nm, molecules feel a deeper trapping potential than atoms. This results in a sudden increase of the potential energy as atoms associate and form molecules (see Fig.2.a). Immediately after production, the effective temperature of molecules is 2.80(6) μ K, while the temperature of Na atoms is 2.42(3) μ K. As molecules thermalize with Na atoms and a hot fraction of atoms evaporates out of the trap, the temperatures of both particles settle to 2.23(6) μ K (see Methods for molecular thermometry).

While this initial settling of temperatures hints at sympathetic cooling, we are able to see much stronger effects by forced cooling and heating of Na atoms. We evaporate Na atoms with almost no loss of molecules by taking advantage of the particles' different polarizabilities: $\alpha_{\text{NaLi}}/\alpha_{\text{Na}} = (m\omega^2)_{\text{NaLi}}/(m\omega^2)_{\text{Na}} \approx 2.6$, where α_i is the polarizability of particle i , ω is an angular frequency for

oscillation in the trap, and m is a particle mass. Fig.2.c shows a curve of thermalization between molecules and atoms beginning with a larger temperature difference after an exponential evaporative cooling ramp followed by a recompression of the trap. As we hold the particles in the trap, their temperatures approach each other. Due to the large particle number ratio, $N_{\text{Na}}/N_{\text{NaLi}} \approx 7$, molecule temperature decreases by $0.68(9) \mu\text{K}$ after thermalization while the temperature of Na atoms only increases by $70(30) \text{ nK}$. However, when the Na is removed immediately before the hold time, the molecule temperature remains fixed during the same period.

As further evidence of thermalization, sympathetic heating of molecules with hot atoms is shown in Fig.3. We first prepare the atom-molecule mixture fully thermalized at $1.5 \mu\text{K}$ after an exponential evaporative ramp in 10 ms followed by a recompression of the trap in 200 ms to the initial trap power of 1.5 W ($50 \mu\text{K}$ trap depth). Then we selectively heat the atoms to $2.07(5) \mu\text{K}$ by sinusoidally modulating the trap amplitude at twice the sodium trap frequency ($2\omega_{\text{Na}} = 2\pi \times 920 \text{ Hz}$) with modulation amplitude of 20% of the trap depth for 100 ms . After 200 ms , particles thermalize and the molecule temperature rises to the temperature of the heated Na atoms. When the trap amplitude is modulated in the same manner without the Na atoms, the temperature of molecules remains at $1.59(5) \mu\text{K}$. The heating process for sodium also induces center of mass motion and breathing oscillations that cause the Na density to depend on time in the early stages of sympathetic heating, which is the reason for the delay in heating and non-exponential thermalization curve.

To quantitatively measure the rate of thermalization, we return to the cleaner situation of

cooling in Fig.2. We fit the temperature to a simple exponential model,

$T(t) = (T_0 - T_\infty) \exp(-\Gamma_{\text{th}} t) + T_\infty$, and obtain $\Gamma_{\text{th}} = 26(7) \text{ s}^{-1}$. Considering that thermalization requires $\approx 3/\xi$ collisions (for Na-NaLi, $\xi \approx 1$, see Methods), we obtain the average elastic collision rate per particle, Γ_{el} , from the measured thermalization rate: $\Gamma_{\text{el}} \approx (3/\xi)\Gamma_{\text{th}} = 80(20) \text{ s}^{-1}$. In the presence of Na atoms, the loss rate of molecules is $\Gamma_{\text{inel}} = 1.29(7) \text{ s}^{-1}$ from a fit to the exponential loss model, $N(t) = N_0 \exp(-\Gamma_{\text{inel}} t)$, (the red-dashed line in Fig.2.b), given a large imbalance of particle numbers ($N_{\text{Na}}/N_{\text{NaLi}} \approx 7$). Comparing the average elastic collision rate to the total loss rate, we obtain the ratio of elastic to inelastic collisions for NaLi, $\gamma \gtrsim \Gamma_{\text{el}}/\Gamma_{\text{inel}} = 62(16)$. Without Na atoms, the molecular loss follows a two-body loss model, $N(t) = N_0/(\beta t + 1)$, (the blue-solid line in Fig.2.b) from which we obtain an initial loss rate of $\beta = 1.02(10) \text{ s}^{-1}$. Regarding the difference between Γ_{inel} and β as an effective inelastic loss rate for collisions between Na and NaLi, we obtain the ratio of “good to bad” collisions, $\gamma \approx \Gamma_{\text{el}}/(\Gamma_{\text{inel}} - \beta) \approx 300$ with an uncertainty of 50%. The Na-NaLi loss rate constant is $4.0 \pm 1.8 \times 10^{-13} \text{ cm}^3/\text{s}$. This is more than two orders of magnitude smaller than the universal loss model rate constant for Na-NaLi s -wave collisions³⁷, which is $1.7 \times 10^{-10} \text{ cm}^3/\text{s}$ (see Methods). While Na-NaLi in their upper stretched states form a stable mixture as shown, preparing Na atoms in their lowest hyperfine state ($|F, m_F\rangle = |1, 1\rangle$) gives a loss rate consistent with the universal loss model²³.

We consider two different evaporation ramps described in Fig.4. The resulting molecule numbers, temperatures, and PSDs from these ramps are displayed in Fig.5. For a single-species system with losses, optimal evaporation can be achieved by a single, continuous decrease of the trap depth. We achieve an increase in PSD by a factor of 7 using a single stage of evaporation

(Fig.4.a and red squares in Fig.5.). This increase is limited by the low initial Na density. In our system, thermalization is dominated by the Na density, while loss is dominated by the NaLi density. In order to overcome the low Na density, we shorten the initial evaporation + recompression cycle ((1)+(2) in Fig.4.b). This cools the Na atoms and quickly increases the density of the cold Na for fast thermalization. After the cold, dense Na efficiently pre-cools the molecules during a short hold of 30 ms in the tight trap (3), we apply the second evaporation ramp (4). In this double evaporation, we achieve a peak PSD of $2.0(4) \times 10^{-2}$ (blue circles in Fig.5.), which is 20 times higher than the initial PSD. Before the final recompression of the trap, the lowest temperature of the molecules is 220(20) nK.

With Na present, more molecules survive the evaporation sequence as we evaporate Na atoms to lower trap depth. This is mainly due to the suppressed two-molecule loss. The loss-rate constant scales linearly with temperature due to the p -wave character of the collisions³⁷. Evaporation to too low trap depth decreases the Na density, which in turn makes the sympathetic cooling of molecules inefficient and anti-evaporation since the molecular loss dominates. This appears as the temperature curving up below a trap power of 0.17 W (5.7 μ K trap depth) for a single stage of evaporation, or 0.14 W (4.5 μ K trap depth) for two-stage evaporation. Without Na, the ramp down in trap depth, (i), is adiabatic to a trap power around 0.3 W, as evidenced by the constant molecule numbers and temperatures. Below that trap power, the ramp down starts becoming non-adiabatic. As a result, a hot fraction of molecules escape, and both molecule number and temperature start decreasing. Note that since fermionic molecules do not thermalize by themselves, this temperature should be regarded as the average kinetic energy of molecules that are not in thermal equilibrium.

The favorable collisional properties of the Na-NaLi mixture in fully stretched states result from strong suppression of electronic spin flips during collisions, which could otherwise lead to fast reactive or inelastic losses. In fully stretched states, direct spin exchange is forbidden and residual spin flips can occur only by weaker interactions. The major contribution would be from dipolar relaxation due to the coupling between the magnetic dipole moments of the spins of Na and NaLi. Studies in other spin-polarized systems ^{17,35,38} predict spin flips through electrostatic interaction at short range induced by intramolecular spin-spin and spin-rotation couplings to be weaker. Dipolar relaxation can be eliminated by using the strong-field seeking stretched state but this was not necessary in our work. It is possible that Na-NaLi is favorable due to the low molecular and reduced masses and smallness of relativistic effects which result in a large rotational constant ^{33,39}, low density of states ²⁹ and small spin-orbit coupling ⁴⁰, respectively. Further, ref. ³² has shown that intramolecular spin-spin coupling causes spin flips for triplet NH molecules, thwarting evaporative cooling. Our results show a clear need for further work to predict which other molecules—and in what conditions of internal states and external fields—will be suitable for collisional cooling at ultracold temperatures.

Technical upgrades to our machine should allow cooling into the quantum degenerate regime by increasing the initial Na density. The dominant loss mechanism, *p*-wave collisions between molecules, will slow down compared to thermalization at lower temperatures, improving the efficiency of cooling. Further, the atomic and molecular states used in this work are magnetically trappable. Magnetic trapping would allow for much larger samples with perfect spin-polarization. This would also eliminate the major concern of molecular loss induced by trapping light ³⁰, mak-

ing NaLi an ideal system for studying quantum chemistry. Concerns about the possibility of sticky collisions ²⁹, which become worse with increasing density of states, have led to pessimism over the prospects for collisional cooling of ultracold molecules. This work demonstrates that sticky collisions do not limit NaLi and probably other low mass systems, suggesting a bright future for cooling light molecules.

References

1. Anderson, M. H., Ensher, J. R., Matthews, M. R., Wieman, C. E. & Cornell, E. A. Observation of bose-einstein condensation in a dilute atomic vapor. *Science* **269**, 198–201 (1995).
2. Davis, K. B. *et al.* Bose-einstein condensation in a gas of sodium atoms. *Phys. Rev. Lett.* **75**, 3969–3973 (1995).
3. Bloch, I., Dalibard, J. & Zwerger, W. Many-body physics with ultracold gases. *Rev. Mod. Phys.* **80**, 885–964 (2008).
4. Baranov, M. A., Dalmonte, M., Pupillo, G. & Zoller, P. Condensed matter theory of dipolar quantum gases. *Chemical Reviews* **112**, 5012–5061 (2012). PMID: 22877362,
5. DeMille, D. Quantum computation with trapped polar molecules. *Phys. Rev. Lett.* **88**, 067901 (2002).
6. Carr, L. D., DeMille, D., Krems, R. V. & Ye, J. Cold and ultracold molecules: science, technology and applications. *New Journal of Physics* **11**, 055049 (2009).
7. Christen, W., Rademann, K. & Even, U. Efficient cooling in supersonic jet expansions of supercritical fluids: CO and CO₂. *The Journal of Chemical Physics* **125**, 174307 (2006).
8. Weinstein, J. D., deCarvalho, R., Guillet, T., Friedrich, B. & Doyle, J. M. Magnetic trapping of calcium monohydride molecules at millikelvin temperatures. *Nature* **395**, 148–150 (1998).

9. Stellmer, S., Pasquiou, B., Grimm, R. & Schreck, F. Laser cooling to quantum degeneracy. *Phys. Rev. Lett.* **110**, 263003 (2013).
10. Hu, J. *et al.* Creation of a bose-condensed gas of ^{87}Rb by laser cooling. *Science* **358**, 1078–1080 (2017).
11. Soldán, P. & Hutson, J. M. Interaction of $\text{NH}(x^3\Sigma^-)$ molecules with rubidium atoms: Implications for sympathetic cooling and the formation of extremely polar molecules. *Phys. Rev. Lett.* **92**, 163202 (2004).
12. Elioff, M. S., Valentini, J. J. & Chandler, D. W. Subkelvin cooling no molecules via "billiard-like" collisions with argon. *Science* **302**, 1940–1943 (2003).
13. Henson, A. B., Gersten, S., Shagam, Y., Narevicius, J. & Narevicius, E. Observation of resonances in penning ionization reactions at sub-kelvin temperatures in merged beams. *Science* **338**, 234–238 (2012).
14. Skomorowski, W. *et al.* Interaction between LiH molecule and Li atom from state-of-the-art electronic structure calculations. *The Journal of Chemical Physics* **134**, 114109 (2011).
15. González-Martínez, M. L. & Hutson, J. M. Ultracold hydrogen atoms: A versatile coolant to produce ultracold molecules. *Phys. Rev. Lett.* **111**, 203004 (2013).
16. Lim, J., Frye, M. D., Hutson, J. M. & Tarbutt, M. R. Modeling sympathetic cooling of molecules by ultracold atoms. *Phys. Rev. A* **92**, 053419 (2015).

17. Morita, M., Kosicki, M. B., Żuchowski, P. S. & Tscherbul, T. V. Atom-molecule collisions, spin relaxation, and sympathetic cooling in an ultracold spin-polarized $\text{Rb}(^2S) - \text{SrF}(^2\Sigma^+)$ mixture. *Phys. Rev. A* **98**, 042702 (2018).
18. Augustovčová, L. D. & Bohn, J. Ultracold collisions of polyatomic molecules: CaOH . *arXiv:1906.09643* (2019).
19. Stuhl, B. K. *et al.* Evaporative cooling of the dipolar hydroxyl radical. *Nature* **492**, 396 (2012).
20. Reens, D., Wu, H., Langen, T. & Ye, J. Controlling spin flips of molecules in an electromagnetic trap. *Phys. Rev. A* **96**, 063420 (2017).
21. Segev, Y. *et al.* Collisions between cold molecules in a superconducting magnetic trap. *arXiv:1902.04549* (2019).
22. Ni, K.-K. *et al.* A high phase-space-density gas of polar molecules. *Science* **322**, 231–235 (2008).
23. Rvachov, T. M. *et al.* Long-lived ultracold molecules with electric and magnetic dipole moments. *Phys. Rev. Lett.* **119**, 143001 (2017).
24. Barry, J. F., McCarron, D. J., Norrgard, E. B., Steinecker, M. H. & DeMille, D. Magneto-optical trapping of a diatomic molecule. *Nature* **512**, 286 (2014).
25. Anderegg, L. *et al.* Radio frequency magneto-optical trapping of CaF with high density. *Phys. Rev. Lett.* **119**, 103201 (2017).
26. Truppe, S. *et al.* Molecules cooled below the doppler limit. *Nature Physics* **13**, 1173 (2017).

27. Collopy, A. L. *et al.* 3-D magneto-optical trap of yttrium monoxide. *Phys. Rev. Lett.* **121**, 213201 (2018).
28. Żuchowski, P. S. & Hutson, J. M. Reactions of ultracold alkali-metal dimers. *Phys. Rev. A* **81**, 060703 (2010).
29. Mayle, M., Quémener, G., Ruzic, B. P. & Bohn, J. L. Scattering of ultracold molecules in the highly resonant regime. *Phys. Rev. A* **87**, 012709 (2013).
30. Christianen, A., Zwierlein, M. W., Groenenboom, G. C. & Karman, T. Trapping laser excitation during collisions limits the lifetime of ultracold molecules. *arXiv: 1905.06846* (2019).
31. Myatt, C. J., Burt, E. A., Ghrist, R. W., Cornell, E. A. & Wieman, C. E. Production of two overlapping Bose-einstein condensates by sympathetic cooling. *Phys. Rev. Lett.* **78**, 586–589 (1997).
32. Janssen, L. M. C., van der Avoird, A. & Groenenboom, G. C. Quantum reactive scattering of ultracold $\text{NH}(x^3\Sigma^-)$ radicals in a magnetic trap. *Phys. Rev. Lett.* **110**, 063201 (2013).
33. Krems, R. V. & Dalgarno, A. Quantum-mechanical theory of atom-molecule and molecular collisions in a magnetic field: Spin depolarization. *The Journal of Chemical Physics* **120**, 2296–2307 (2004).
34. Zuchowski, P. S. & Hutson, J. M. Cold collisions of $\text{N}(^4S)$ atoms and $\text{NH}(^3\Sigma)$ molecules in magnetic fields. *Phys. Chem. Chem. Phys.* **13**, 3669–3680 (2011).

35. Tscherbul, T. V., Kłos, J. & Buchachenko, A. A. Ultracold spin-polarized mixtures of $^2\Sigma$ molecules with s -state atoms: Collisional stability and implications for sympathetic cooling. *Phys. Rev. A* **84**, 040701 (2011).
36. Heo, M.-S. *et al.* Formation of ultracold fermionic NaLi feshbach molecules. *Phys. Rev. A* **86**, 021602 (2012).
37. Idziaszek, Z. & Julienne, P. S. Universal rate constants for reactive collisions of ultracold molecules. *Phys. Rev. Lett.* **104**, 113202 (2010).
38. Hummon, M. T. *et al.* Cold N+NH collisions in a magnetic trap. *Phys. Rev. Lett.* **106**, 053201 (2011).
39. Campbell, W. C. *et al.* Mechanism of collisional spin relaxation in $^3\Sigma$ molecules. *Phys. Rev. Lett.* **102**, 013003 (2009).
40. Warehime, M. & Kłos, J. Nonadiabatic collisions of CaH with Li: Importance of spin-orbit-induced spin relaxation in spin-polarized sympathetic cooling of CaH. *Phys. Rev. A* **92**, 032703 (2015).

Figure 1. Experimental setup. The Na atoms (yellow circles) and NaLi molecules (yellow and red circles on black sticks) are trapped in a 1D optical lattice formed by a 1596 nm laser, which is retro-reflected. The magnetic field, which defines the quantization axis, is coaxial with the lattice beam. The leftover free atoms after the formation of the ground-state molecules are removed by resonant light in the radial direction (y -axis in figure). STIRAP is performed with beams that propagate along the axial direction (z -axis in figure). The ground-state molecules are detected by absorption imaging of the dissociated atoms along the axial direction.

Figure 2. Thermalization of Na and NaLi. **a**, The trapping potential of molecules (the red-solid line) is deeper than that of Na atoms (the black-dashed line). This allows us to evaporate Na atoms with negligible loss of molecules. The molecule number (**b**) and temperature (**c**) are measured at various hold times after an exponential evaporation ramp to a trap power of 0.21 W (7 μ K trap depth) in 100 ms followed by a recompression to 1.2 W (40 μ K trap depth) in 10 ms. In the number plot, **b**, the red-dashed line is an exponential loss fit and the blue-solid one is a two-body loss fit (details in main text). The dashed line in the temperature plot, **c**, is an exponential fit. Note that a drop in temperature does not occur in the absence of Na atoms. The exponential fit of the molecule's temperature agrees well with the measurement, but should be regarded as an interpolation to determine the initial slope of the thermalizaion. For this measurement, Na number $\approx 1.5 \times 10^5$. Each error bar represents the uncertainty of the mean estimated from a fit error and a statistical error corresponding to 1 standard deviation of 3-8 measurements. This definition of the error bar holds throughout the article.

Figure 3. Sympathetic heating. After forced heating of Na atoms (see main text for details), the molecule temperature (red squares) rises and reaches to the Na temperature (black asterisk) as both particles thermalize. Note that the temperature of molecules without the hot atoms (blue circles) remains cold. Error bars are estimated from 4 measurements.

Figure 4. Evaporation sequences. The initial power of the 1596 nm trapping laser is 1.5 W. At the end of evaporation we recompress the trap to the initial power to increase thermalization rate and for a straightforward comparison of density without re-scaling the trap volume. **a**, Single evaporation consists of (i) 100 ms exponential forced evaporation ($\tau = 40$ ms), where trap depth, $U(t) = A \exp(-t/\tau) + B$, (ii) 500 ms recompression, and (iii) 40 ms hold for complete thermalization. **b**, Double evaporation consists of (1) 100 ms exponential forced evaporation ($\tau = 40$ ms), (2) 50 ms recompression to the initial trap depth, (3) 30 ms hold, (4) 300 ms exponential evaporation ($\tau = 120$ ms), and (5) 200 ms recompression.

Figure 5. Increasing phase-space density. The molecule number (**a**), temperature (**b**), and PSD (**c**) are plotted versus the power of the 1596 nm trapping laser at the end of the forced exponential evaporation: (i) for single evaporation and (1) for double evaporation (see Fig.4.). For the double evaporation, we ramp the power down to 0.06 W (2 μ K trap depth) in (4), the lowest point that gives a molecular signal high enough for consistent temperature measurement. Evaporation to this low trap depth in a single stage of evaporation leads to loss of almost every molecule. The black-dashed lines in **b**, **c** indicate the molecule temperature and PSD after STIRAP and removal of free atoms (shaded areas show ± 1 error bar). This PSD corresponds to $2.6(1) \times 10^4$ molecules. Note

that when Na atoms are not in the trap or the evaporation is not performed to sufficiently low trap depth, the PSD is lower than the initial value. This is mainly due to the molecular two-body loss. The solid curves are to guide the eye. Error bars are estimated from 4-9 measurements.

Methods

Atomic sample preparation We produce an ultracold mixture of ^{23}Na and ^6Li in their upper stretched hyperfine states (in the $|F, m_F\rangle$ basis, these states correspond to $|2, 2\rangle$ for Na and $|3/2, 3/2\rangle$ for Li) in an Ioffe-Pritchard magnetic trap at a bias field of 2 G. We cool the Na atoms using microwave-induced evaporation and sympathetically cool the Li atoms with the Na atoms^{31,41–43}. Then, the mixture is transferred into the combination of two coaxial optical traps: a 1064 nm optical dipole trap (30 μm waist, 10 W power) and a 1596 nm 1D optical lattice (50 μm waist, 2 W power). After 0.6 seconds of forced evaporation in the 1064 nm optical dipole trap, the trap is switched off. Then, in a 1596 nm 1D lattice, the sample is transferred to the lowest-energy Zeeman states (in the $|F, m_F\rangle$ basis, $|1, 1\rangle$ for Na, and $|1/2, 1/2\rangle$ for Li) through a Landau-Zener magnetic field sweep. By controlling the microwave power for the Landau-Zener sweep, we intentionally leave a fraction of Na atoms in the upper stretched hyperfine state for later use as coolants of the NaLi molecules.

Molecule formation and detection As previously demonstrated with other atomic species^{22,23,44–51}, NaLi ground state molecules are created from Feshbach molecules in the least-bound vibrational state. In a 1596 nm 1D optical lattice, NaLi Feshbach molecules form in the $a^3\Sigma^+$, $v = 10$, $N = 2$, $m_N = -2$ state from the atoms in the lowest-energy Zeeman states by sweeping the magnetic field across an interspecies scattering resonance ("Feshbach resonance") at 745 G³⁶ (v and N are the vibrational and rotational molecular quantum numbers, respectively). Then, $\approx 98\%$ of Feshbach molecules are transferred to the triplet ground state ($a^3\Sigma^+$, $v = 0$, $N = 0$) by means of a 30 μs long STIRAP sequence with the intermediate state ($v = 11$, $N = 1$, $m_N = -1$) in

the $c^3\Sigma^+$ excited potential. Use of 1596 nm light for the trap improves the lifetime of the NaLi molecules by suppressing spontaneous photon scattering compared to the more common 1064 nm trap. The 1D lattice provides strong axial confinement to overcome the anti-trapping produced by magnetic curvature²³. The STIRAP light (upleg: 833 nm [360.00381(1) THz], downleg: 819 nm [366.23611(1) THz]^{23,52,53}) is obtained from two home-built external cavity diode lasers (ECDL)⁵⁴ locked to an ultra-low-expansion cavity. The relative linewidth of the two ECDLs is less than 1 kHz. In order to attain sufficient optical power for the upleg transition, we use a 500mW high-power laser diode injection-locked by 2mW of ECDL light. After molecule formation, a resonant light pulse is applied for 1 ms to remove the free atoms that were not converted to molecules. These atoms in the lowest-energy Zeeman states make the loss of NaLi fast, at roughly the universal loss model rate²³. Sodium atoms in this state are optically pumped by the resonant removal light into a dark Zeeman state ($|F, m_F\rangle = |2, 1\rangle$). Adding a repump beam to address this state removes the need to drop the magnetic field to blast the atoms at low field, which caused significant heating and loss of the molecules in our previous work²³. We detect ground-state molecules by reverse STIRAP and a magnetic field sweep across the Feshbach resonance followed by resonant absorption imaging of the resulting free atoms.

Thermometry of molecules In order to avoid issues with different atomic and molecular trapping potentials, we dissociate molecules in free space after turning off the trap, which allows accurate molecular thermometry. Since the particle velocities are fixed after the trap is turned off, the density at some time-of-flight maps the velocity distribution of molecules in the trap. The molecule temperature is determined from a fit to such density profiles. Extra kinetic energy could be added in

quadrature while Feshbach molecules dissociate into atomic continuum states⁵⁵. We determine the parameters of Feshbach dissociation (i.e., the rate of magnetic field sweep) in order to minimize the released dissociation energy. All uncertainties quoted in this article are from statistical errors and fit errors. The systematic uncertainty, which is mainly determined by the imaging magnification, is $\approx 6\%$ but has no effect on measured thermalization rates since it gives a common multiplier to all temperature measurements.

Na-NaLi *s*-wave elastic scattering cross-section The elastic scattering rate between Na and NaLi is given by $\Gamma_{\text{el}} = n_{\text{ov}} \sigma_{\text{el}} v_{\text{rel}}$ where n_{ov} is the overlap averaged density of the mixture, σ_{el} is the elastic scattering cross-section, and v_{rel} is the mean relative velocity⁵⁶:

$$v_{\text{rel}} = \sqrt{\frac{8k_B}{\pi} \left(\frac{T_{\text{Na}}}{m_{\text{Na}}} + \frac{T_{\text{NaLi}}}{m_{\text{NaLi}}} \right)}$$

$$n_{\text{ov}} = \frac{I}{\frac{N_{\text{Na}} N_{\text{NaLi}}}{N_{\text{Na}} + N_{\text{NaLi}}}} = \frac{N_{\text{Na}} N_{\text{NaLi}} \bar{\omega}_{\text{Na}}^3 \left[\left(\frac{2\pi k_B T_{\text{Na}}}{m_{\text{Na}}} \right) \left(1 + \frac{\alpha_{\text{Na}}}{\alpha_{\text{NaLi}}} \frac{T_{\text{NaLi}}}{T_{\text{Na}}} \right) \right]^{-\frac{3}{2}}}{\frac{N_{\text{Na}} N_{\text{NaLi}}}{N_{\text{Na}} + N_{\text{NaLi}}}} \quad (1)$$

where m_i , T_i , and α_i represent the mass, temperature, and polarizability of the particle i respectively, $I = \int dV n_{\text{Na}} n_{\text{NaLi}}$ is the density overlap integral of the mixture in a harmonic trap, and $\bar{\omega}_{\text{Na}} = (\omega_x \omega_y \omega_z)^{1/3} = 2\pi \times (540 \cdot 410 \cdot 34000)^{1/3}$ Hz is the geometric mean of the trap frequencies. The differential gravitational sag between molecules and atoms has a negligible effect on the overlap density. The effective number of particles per lattice site, $N_{(\text{Na}, \text{NaLi})}$, is the total number of particles divided by a factor l_{eff}/a , where $a = \lambda/2$ is the lattice spacing and l_{eff} is the effective axial width (in the z -direction, see Fig.1.) of the atomic density distribution across all lattice sites:

$$l_{\text{eff}} = 2 \frac{\int_0^\infty z \exp(-z^2/2\sigma^2) dz}{\int_0^\infty \exp(-z^2/2\sigma^2) dz} = \sqrt{\frac{8}{\pi}} \sigma, \quad (2)$$

where $\sigma = 0.72(1)$ mm is the Gaussian width from a fit of the atomic density profile.

In a mass-imbalanced system, the factor $3/\xi$ quantifies the approximate average number of collisions per particle required for thermalization, where $\xi = 4m_{\text{Na}}m_{\text{NaLi}}/(m_{\text{Na}} + m_{\text{NaLi}})^2$ ⁴². For the Na-NaLi mixture, this corresponds to approximately 3 collisions since the mass difference is small. Thus, the relation between the thermalization rate and the elastic scattering rate is given by $\Gamma_{\text{th}} \approx \Gamma_{\text{el}}/(3/\xi)$. In our system, where the particle number is largely imbalanced (i.e., $N_{\text{Na}}/N_{\text{NaLi}} \approx 7$), we can write the thermalization rate as

$$\Gamma_{\text{th}} \approx \frac{(I/N_{\text{NaLi}})\sigma_{\text{el}}v_{\text{rel}}}{3/\xi}, \quad (3)$$

where I/N_{NaLi} is the average density of Na atoms seen by NaLi molecules. Given the measured thermalization rate, we obtain the elastic scattering cross-section between a molecule and an atom, $\sigma_{\text{el}} \approx (3/\xi)(N_{\text{NaLi}}/v_{\text{rel}}I)\Gamma_{\text{th}} = 2.4(6) \times 10^{-11}\text{cm}^2$ and the corresponding scattering length, $a = 263(66)a_0$ where a_0 is the Bohr radius.

In addition to the simple exponential fit, we perform a numerical simulation of the thermalization process based on the differential equation for $\Delta T = T_{\text{NaLi}} - T_{\text{Na}}$ ^{42,43,56}:

$$\frac{1}{\Delta T} \frac{d(\Delta T)}{dt} = -\Gamma_{\text{th}} = -\frac{\xi}{3}n_{\text{ov}}\sigma_{\text{el}}v_{\text{rel}}. \quad (4)$$

In the numerical simulation, the temperature dependence of n_{ov} , σ_{el} , and v_{rel} is fully taken into account. The s -wave elastic scattering cross-section between Na and NaLi is given by $\sigma_{\text{el}} = \frac{4\pi a^2}{[1 - (1/2)k^2 r_0 a^2] + (ka)^2}$, where $\hbar k = \mu v_{\text{rel}}$ is the relative momentum (μ is the reduced mass) and r_0 is the effective range calculated from the scattering length, a and $C_6^{\text{Na-NaLi}}$ (see “Na-NaLi loss rate constant from the universal loss model” below). We iteratively solve eq. (4) by varying a ,

and found the optimal solution that minimizes the weighted sum of squared residuals: $\sum_i ((\Delta T_{e,i} - \Delta T_{n,i})/\sigma_{\Delta T_{e,i}})^2$, where the subscript n denotes the numerical solution, e denotes the measurement, and $\sigma_{\Delta T_{e,i}}$ is the standard deviation of the measurement at i^{th} time step. The numerical solution for a obtained in this way agrees with the result calculated from the simple exponential model above within the uncertainty.

Na-NaLi loss rate constant The Na-NaLi loss rate constant is defined as the differential loss rate, $(\Gamma_{\text{inel}} - \beta)$, normalized by the density of Na overlapped with NaLi (i.e., the overlap averaged density of the mixture, n_{ov}), where Γ_{inel} is the molecular loss rate with Na and β is without Na. As shown in the calculation of the s -wave elastic scattering cross-section between Na and NaLi, $n_{\text{ov}} \approx (I/N_{\text{NaLi}})$ given the large imbalance of particle numbers. Thus, the Na-NaLi loss rate constant in the main text is calculated from $(\Gamma_{\text{inel}} - \beta)/(I/N_{\text{NaLi}})$.

Na-NaLi loss rate constant from the universal loss model We compare the measured loss rate constant between Na and NaLi with the theoretical prediction based on the universal loss model³⁷. When calculating the theoretical loss rate constant, we estimate the van der Waals coefficient, $C_6^{\text{Na-NaLi}}$ between Na and NaLi as the sum of C_6 's for atomic pairs that constitute the collision partners using values from ref.⁵⁷: $C_6^{\text{Na-NaLi}} = C_6^{\text{Na-Li}} + C_6^{\text{Na-Na}}$.

41. Hadzibabic, Z. *et al.* Fiftyfold improvement in the number of quantum degenerate fermionic atoms. *Phys. Rev. Lett.* **91**, 160401 (2003).

42. Mosk, A. *et al.* Mixture of ultracold lithium and cesium atoms in an optical dipole trap.

Applied Physics B **73**, 791–799 (2001).

43. Ivanov, V. V. *et al.* Sympathetic cooling in an optically trapped mixture of alkali and spin-singlet atoms. *Phys. Rev. Lett.* **106**, 153201 (2011).
44. Lang, F., Winkler, K., Strauss, C., Grimm, R. & Denschlag, J. H. Ultracold triplet molecules in the rovibrational ground state. *Phys. Rev. Lett.* **101**, 133005 (2008).
45. Danzl, J. G. *et al.* An ultracold high-density sample of rovibronic ground-state molecules in an optical lattice. *Nature Physics* **6**, 265 (2010).
46. Takekoshi, T. *et al.* Ultracold dense samples of dipolar RbCs molecules in the rovibrational and hyperfine ground state. *Phys. Rev. Lett.* **113**, 205301 (2014).
47. Molony, P. K. *et al.* Creation of ultracold $^{87}\text{Rb}^{133}\text{Cs}$ molecules in the rovibrational ground state. *Phys. Rev. Lett.* **113**, 255301 (2014).
48. Park, J. W., Will, S. A. & Zwierlein, M. W. Ultracold dipolar gas of fermionic $^{23}\text{Na}^{40}\text{K}$ molecules in their absolute ground state. *Phys. Rev. Lett.* **114**, 205302 (2015).
49. Guo, M. *et al.* Creation of an ultracold gas of ground-state dipolar $^{23}\text{Na}^{87}\text{Rb}$ molecules. *Phys. Rev. Lett.* **116**, 205303 (2016).
50. Yang, H. *et al.* Observation of magnetically tunable feshbach resonances in ultracold $^{23}\text{Na}^{40}\text{K}$ + ^{40}K collisions. *Science* **363**, 261–264 (2019).
51. Seeßelberg, F. *et al.* Extending rotational coherence of interacting polar molecules in a spin-decoupled magic trap. *Phys. Rev. Lett.* **121**, 253401 (2018).

52. Rvachov, T. M. *et al.* Photoassociation of ultracold NaLi. *Phys. Chem. Chem. Phys.* **20**, 4746–4751 (2018).
53. Rvachov, T. M. *et al.* Two-photon spectroscopy of the NaLi triplet ground state. *Phys. Chem. Chem. Phys.* **20**, 4739–4745 (2018).
54. Cook, E. C., Martin, P. J., Brown-Heft, T. L., Garman, J. C. & Steck, D. A. High passive-stability diode-laser design for use in atomic-physics experiments. *Review of Scientific Instruments* **83**, 043101 (2012).
55. Mukaiyama, T., Abo-Shaeer, J. R., Xu, K., Chin, J. K. & Ketterle, W. Dissociation and decay of ultracold sodium molecules. *Phys. Rev. Lett.* **92**, 180402 (2004).
56. Ravensbergen, C. *et al.* Production of a degenerate fermi-fermi mixture of dysprosium and potassium atoms. *Phys. Rev. A* **98**, 063624 (2018).
57. Derevianko, A., Babb, J. F. & Dalgarno, A. High-precision calculations of van der waals coefficients for heteronuclear alkali-metal dimers. *Phys. Rev. A* **63**, 052704 (2001).

Data availability The data that support the findings of this study are available from the corresponding author upon reasonable request.

Acknowledgements We thank Martin Zwierlein for useful discussions and Jiangtian Yao for technical assistance. We acknowledge support from the NSF through the Center for Ultracold Atoms and award 1506369, from the NASA Fundamental Physics Program, and from the Samsung Scholarship.

Competing interests The authors declare no competing financial interests.

Corresponding author Correspondence to Hyungmok Son (e-mail: hson@g.harvard.edu)

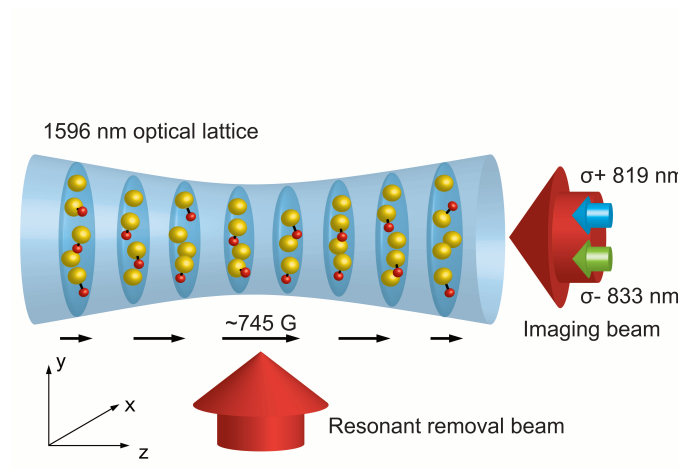


Fig. 1: Experimental set up.

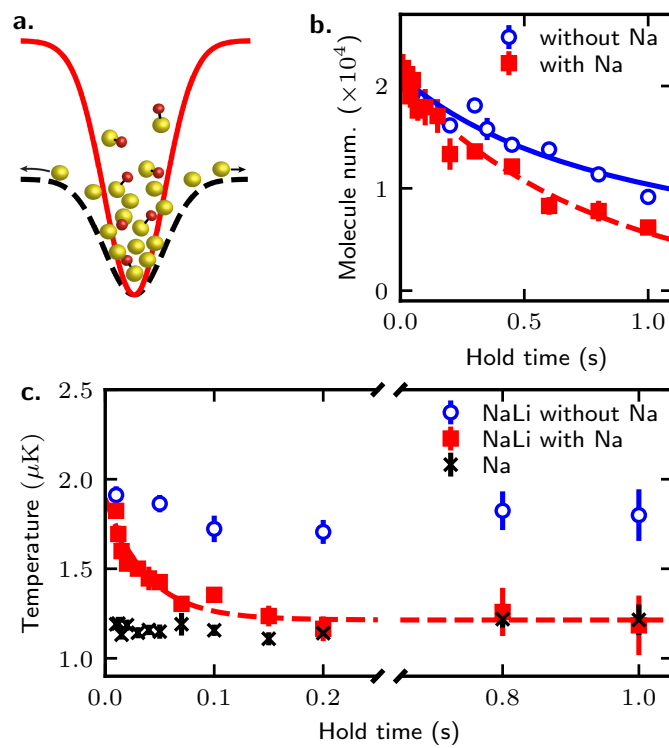


Fig. 2: Thermalization of Na and NaLi.

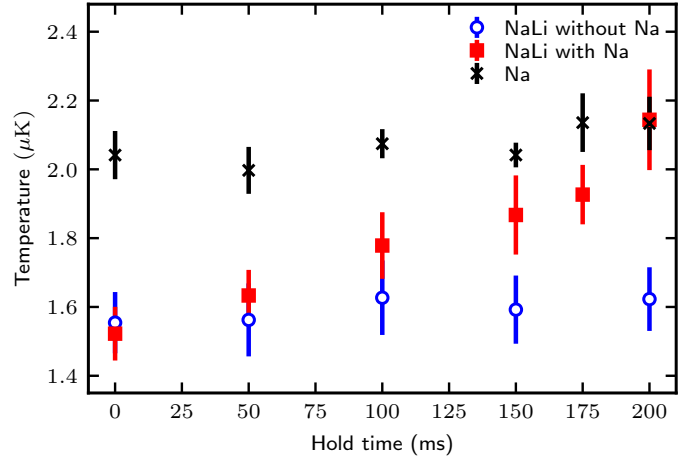


Fig. 3: Sympathetic heating.

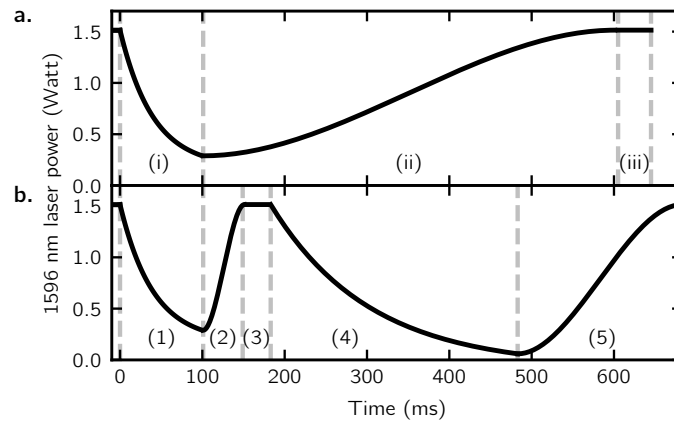


Fig. 4: Evaporation sequences.

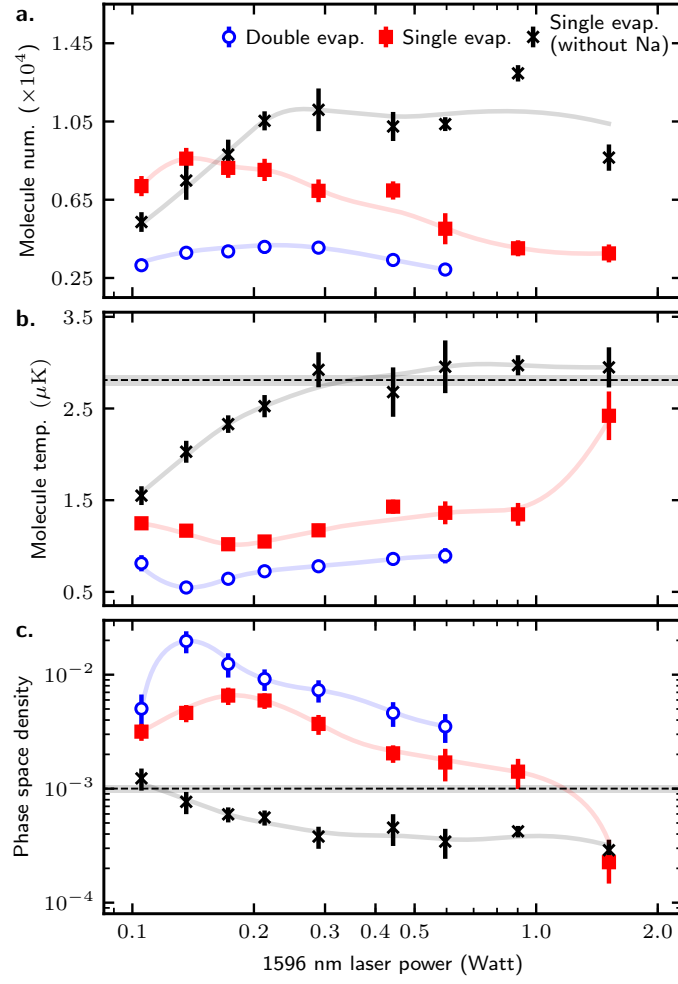


Fig. 5: Increasing phase-space density.